Nuclear Instruments and Methods in Physics Research B52 (1990) 357–365
North-Holland

#5

AMS of heavy ions with small accelerators *

L.R. Kilius, N. Baba, M.A. Garwan, A.E. Litherland, M.-J. Nadeau, J.C. Rucklidge, G.C. Wilson and X.-L. Zhao

IsoTrace Laboratory, University of Toronto, Toronto, Canada

Recent advances in the detection and the routine measurements of heavy elements by accelerator mass spectrometry (AMS) are reviewed. Particular emphasis will be given to the measurement of low energy (≤ 15 MeV) and high-Z ions using small (≤ 3 MV) accelerators.

1. Introduction

Large accelerators [1,2] dominated the early development of accelerator mass spectrometry (AMS) because the ion atomic number could be identified, for all the light ions ^{10}Be, ^{14}C, ^{26}Al and ^{36}Cl, in the energy range 30–80 MeV using gas ionization detectors. The largest accelerator systems were also capable of exploring detection limits for heavier radio-isotopes by stripping all electrons from the atom at energies of 2–10 MeV/nucleon, thereby removing isobaric interferences in selected cases [3]. The ability to resolve atomic number was essential in these early experiments in order to establish the limits of stability for negative ion isobars for which little or no previous data was available. Even in cases, such as the analysis of ^{129}I, for which the isobaric negative ion was known to be unstable, energy-loss measurements or time-of-flight detection were required to compensate for inadequate resolution of the magnetic and electric systems which removed the more abundant stable isotopes. As an optimum charge state could also be chosen on these machines, it was a simple procedure to maximize the rejection of molecular interference and also to maximize the charge state yield and hence acquire low detection limits.

The operational costs of these systems do not always warrant routine analysis beyond the seminal experiments to demonstrate detection feasibility. Recent advances in the control of backgrounds for radio-isotope measurements by AMS have made possible the detection of ^{129}I at 4.5 MeV [4] and the analysis of pure semiconductor metal for trace element content [5] on a 2 MV accelerator. It is expected that other techniques will be developed to make unnecessary the use of high energies for the purpose of isobaric separation. The majority of these advances will undoubtedly exploit the stability of negative atomic [6], molecular ions [7,8] or laser techniques [9].

This paper will focus on the development of heavy-element analysis on small accelerator systems both in terms of the requirements for background reduction and routine analysis. Examples will be taken from measurements on ^{129}I, the platinum group elements (PGE), ^{230}Th and the search for stable negative ions.

2. Detectors for heavy-element analysis

The energy loss associated with the passage of an ion through a variety of gases and solids is governed by the familiar Bethe-Bloch equation [10] which provides a means of identifying the atomic number. Although the energy loss was shown to be proportional to Z_{eff}^2, at low energies and for high-Z atoms the majority of the core electrons shield the nuclear charge so that $Z_{\text{eff}} \propto Z^{1/3} v/v_0$, where $v_0 = e^2/h$ and v is the ion velocity. As the ion passes through the detector, the charge state also fluctuates about a mean value, further reducing the effectiveness of atomic number determination. This screening of the atomic charge does not provide for appreciable differentation between adjacent atomic numbers much beyond $Z = 20$ unless the core electrons are stripped away to make $Z_{\text{eff}} = Z$. In fact, for ion energies of approximately 15 MeV, the rate of energy loss is nearly independent of Z. Therefore the energy loss criteria that enabled isobar separation on large accelerators inhibit the use of the same detectors at low energy and high Z. It is therefore apparent that the unique identification of massive ions will no longer be possible at these low energies and for elements of high atomic number.

A precise measurement of the ion energy is very important if a determination of Z is not possible. A typical tandem accelerator system will generate, and often the analysis system will transmit, molecular fragments that differ in energy from the ion of interest by multiples of M/q unless very high ($M/\Delta M \geq 5000$)

* Invited paper.

0168-583X/90/$03.50

resolution is used. For hydride fragments that are transmitted by the accelerator and spectrometers, the energy resolving power required by the final detector is of the order $M \times q$, M being the ion mass and q the charge state selected. As the best attainable energy resolution for heavy ions at low energies is of the order of one percent, it is unlikely that new detector technology alone will be sufficient to completely resolve all ion masses from their corresponding hydride fragments.

Although a measurement of atomic number would be preferable, the mass of an ion is another signature that can be used in most cases to specify the ion completely. This applies especially to trace element analysis in all cases except for indium where both isotopes have isobaric interferences. Even here as with the radioisotopes, the possible instability of the isobar negative ion, in this case cadmium, can be exploited to overcome the isobar problem.

Time-of-flight (ToF) detectors were used primarily for mass identification of ions of known energy and have been valuable for separating ^{129}I from ^{127}I to the 10^{-14} range. However, the mass resolution of a ToF detector is ultimately constrained by the timing spreads and aberrations. In first order, for a drift length L, the energy straggling contributes a term [11];

$$\Delta L = -\frac{1}{2}\frac{\Delta E}{E}L, \tag{1}$$

which adds a time spread of $\Delta T = \Delta L / V_0$, where V_0 is the ion velocity.

Hence the timing resolution is completely independent of the flight path length within the ToF detector and is limited by the energy spread in eq. (1). For a typical 5.0 μg/cm^2 carbon foil, energy straggling at energies of 10 MeV limits the mass resolving power $(M/\Delta M)$ to approximately 250. Clearly this would be inadequate to resolve the contribution from hydrides as a resolving power of at least $(M+1)\times(q+1)$ is required in this case. Note that the resolving power needed increases linearly with the selected charge state. ToF systems can be built to reduce the timing aberration for both electrostatic [11] or magnetic systems [12]. On the other hand, a combination of electrostatic and magnetic analyzers will also select ion velocity and hence determine M/q without the limitations imposed by ToF and energy detectors. This is the preferred mode of operation for high-Z and low-E ions.

3. A heavy-element AMS system

The design of a low-energy AMS system for heavy ions will be governed by a number of atomic physics problems for heavy-ion transport.

The energy distribution of sputtered ions has been extensively described in the literature for both atoms [13,14] and molecules and has been observed to extend out to the kinematically allowed limit [15]. The higher energy components fall off approximately as $[E_s/E_0(\Delta M/M)]^n$, where n ranges from 2 to 3, E_s is the mean energy of sputtered ions and E_0 is the extracted ion energy. Without an electric analyzer to control the energy distribution of sputtered ions 10^{-4} of the ^{127}I beam will be injected along with the ^{129}I if the E^{-2} fall-off is assumed. This is consistent with the value of 8.3×10^{-4} measured for all ^{127}I ions sputtered from an AgI sample and injected into the accelerator during ^{129}I measurements [15].

Elastic scattering collisions are one of the major causes of background contamination in conventional spectrometer systems and will also have an impact on AMS injection systems. Based on geometrical arguments and the relevant scattering cross sections, the fraction (F) of a primary isotope that scatters from a magnetic spectrometer into the defining slits can be described by [16]:

$$F = 4N\sigma\left(\frac{M}{\Delta M}\right)^{n-1}\Delta X T, \tag{2}$$

where σ is the scattering cross section from N atoms, ΔX the slit width, n is defined by the scattering process and T contains geometric factors.

Although originally developed for positive ions, eq. (2) will apply to negative ions for appropriate σ and n. A typical value for the ^{127}I scattered into the ^{129}I acceptance is $F = 49P$ where P is the system pressure in Torr. At the 10^{-7} Torr range typical to AMS systems the scattering contribution is 170 times lower than the previously observed contribution from sputter tails. Unlike the contribution from the sputtering process, to eliminate scattering, additional analyzers must follow the initial magnet analysis.

Because the classical elastic scattering cross section falls off as $1/E$, we would expect a smaller contribution from elastic scattering at MeV ion energies. Charge changing in the residual gas does however become significant with typical cross sections for ^{127}I of the order 10^{-16} cm^2 [17]. Using eq. (2) with the appropriate modifications to the cross section, a single charge change event (5+ to 6+) will transmit $F \le 4.3\times10^{-5}$ of the incident $^{127}I^{5+}$ ions through the slits as $^{127}I^{6+}$ along with $^{129}I^{5+}$ ions. This must be compared to the 1.4×10^{-10} ^{127}I for elastic scattering at the same energy. A second magnet or electrostatic analyzer could be used to remove the 6+ ions. For an electric analyzer to transmit these ions, an additional charge change-back to charge state 5+ will be required with a corresponding reduction in the transmitted ^{127}I of order F^2.

As molecules pass through solids and to a lesser extent gases, the electron loss process exposes the constituent molecular ions to increased repulsive Coulomb forces. This not only introduces a lateral spread in the

beam but also contributes a fractional energy spread given by $\pm 2\sqrt{\epsilon/E}/(q+1)$, where upon breakup, the fragments have relative motion characterized by an energy ϵ, a final energy E and charge q. For ions that have marginal M/q difference, the resulting spread will prevent any high-resolution system from separating the fragment from the ion of interest.

While the tandem accelerator destroys molecules, it introduces a further complication by producing fragments with M/q and E/q ratios that can be identical to the ion of interest and hence indistinguishable using conventional magnetic and electric analyzers. As a general rule, charge states have to be chosen to avoid these multiples of M/q. For analysis of actinides a well-known example is the multiplet $^{234}U^{6+}$, $^{195}Pt^{5+}$, $^{156}Dy^{4+}$, $^{117}Sn^{3+}$, $^{78}Se^{2+}$ and $^{39}K^{1+}$ which are unresolvable by any combination of analyzers if the mass defects are ignored and are only separable in energy provided that the counting rate from any one element is not excessive.

The problem of injected metastable ions and in particular hydrides is less understood from the perspective of background. Molecules of mass M^-_{4n} that decay into M^-_{2n} are indistinguishable by magnetic analysis from an ion of mass M, although readily eliminated by an electric analyzer. Similarly a hydride MH^-_n that decays to MH^-_{n-m} will approximate closely an ion of mass MH^-_{n-2m}. Metastable ions of this kind can be eliminated by an electric analyzer with resolving power $E/\Delta E$ of $M+2$ as compared to a resolving power $M/\Delta M$ of M^2+2M for a magnet. After acceleration the same fragment requires a resolving power of $(q+1)\times(M+1)$ for both magnetic and electric analyzers. Clearly it is advantageous to eliminate these molecules before acceleration. An ideal spectrometer would locate electric analyzers both before and after a magnetic system to first define the ion energy and then to remove the metastable fragments transmitted by the magnet.

As a result of some of the above considerations, the Tandetrons at IsoTrace and Gif-sur-Yvette have added 45° spherical electric analyzers to their injection systems. The IsoTrace system has been further expanded to permit heavy-element analysis by the addition of a high-resolution ($M/\Delta M = 2600$) high bending power (120 MeV amu) 90° double-focussing magnet and a 45° ($E/\Delta E = 900$) electric analyzer and a quadrupole doublet, fig. 1. This combination of electric and magnetic analyzers has permitted the detection and subsequent measurements on a variety of heavy elements, some of which are highlighted below.

4. ^{129}I detection

The measurement of $^{129}I/^{127}I$ ratios requires only a reduction of ^{127}I at the final detector as xenon is very rare and the ^{129}Xe isobar is eliminated by the use of negative ions. Any ^{127}I must be eliminated completely before entering the final detector as the ^{127}I and ^{129}I will be indistinguishable to energy detectors. The combination of electric and magnetic analyzers prior to injection into the tandem accelerator and after post-acceleration reduces the ^{127}I component due to scattering, charge changing processes and the decay in flight of molecular ions to 1.9×10^{-8} and 4.8×10^{-9}, respectively, for both sides of the acceleration process. This combined rejection of 8×10^{-17} (scattered ions per incident ^{127}I per second) exceeds the anticipated ^{129}I counting rate from natural background materials and make possible $^{129}I/^{127}I$ measurements on small accelerators.

The complete separation of ^{129}I from ^{127}I is illustrated in fig. 2, for a 2% region in momentum around the $^{129}I^{5+}$ region with the energy detector selecting full-energy ions. Three processes are observed to contribute to the ^{127}I residual ions entering the accelerator.

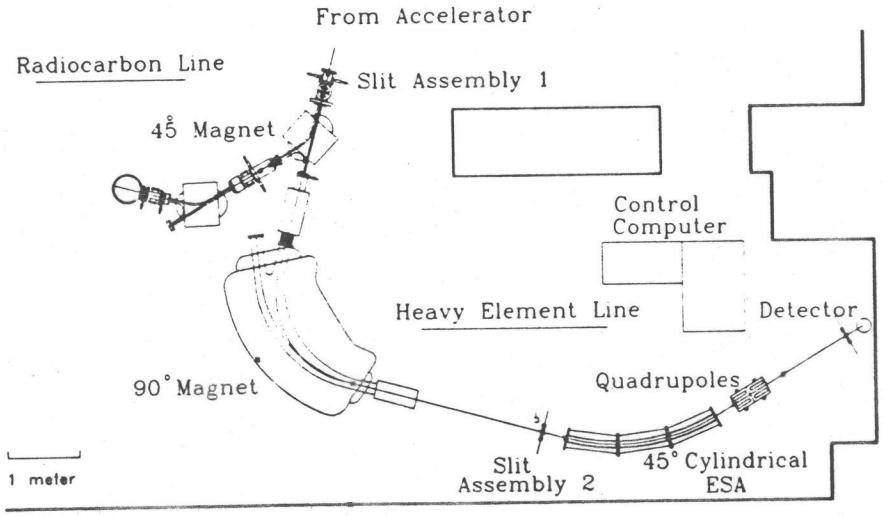

Fig. 1. A schematic representation of the heavy-element analysis system following the tandem accelerator at the IsoTrace laboratory.

The dominant peak, to the lower momentum side of ^{129}I, originates from the sputter tail and to a lesser extent the decay of metastable hydrides and scattering. As mass-129 ions at the extracted ion energy are selected by the combined magnetic and electric analyzer, the smaller of the three ^{127}I ion peaks can only result from the decay in flight of IH_2^{*-} into IH^-. This is not inconsistent with the expected metastability of the hydrogen halides [18] and a partial half-life for the process IH_2^- into IH^- of 14 μs.

Although no counts were observed at the $M = 128$ field setting, a few ions were observed at the magnetic field corresponding to $M = 130$. These ions originate from a much more complex process. Mass-129 molecules of $^{52}CrXY^-$ are created within the ion-source components. For example, $^{52}Cr^{65}Cu^{12}C^-$ is a possible candidate. The destruction of the molecule will produce $^{52}Cr^{2+}$ ions with the required magnetic rigidity for observation at this field setting. The few ions that appear within the energy selection window originate from pileup coincidence from an intense lower energy 2 + beam. The scan was terminated below the peak to avoid damage to the energy detector.

Because of the anthropogenic input of ^{129}I, a wide dynamic range of iodine isotope ratios are observed in the environment. Iodine isotope ratios in pre-bomb marine sediments have been measured in the range of (1.1 to 1.5) $\times 10^{-12}$ [20], while other marine samples have been measured in the range of 3.8×10^{-12} to 2.8×10^{-11}, depending on geographical location. Some of these are summarized in fig. 3 for a selection of pre- and post-bomb biogenic samples and brines [19]. Backgrounds of $(3.9 \pm 1.9) \times 10^{-14}$ $^{129}I/^{127}I$ are consistent with that measured at other AMS facilities for old iodide [20]. There are clear demarcations between the pre- and post-bomb samples. The highest isotopic ratio for measurement number seven corresponds to iodine

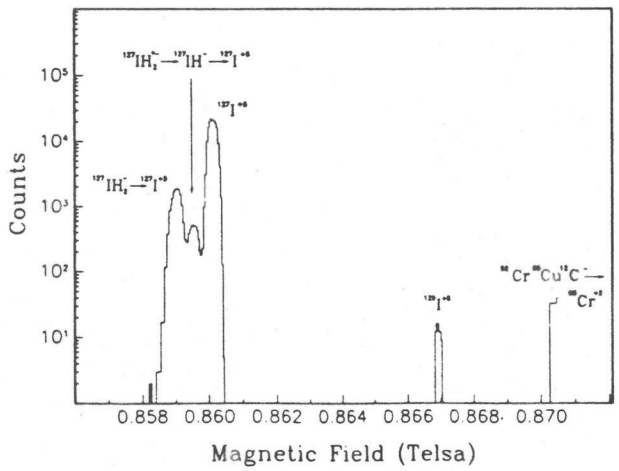

Fig. 2. The particle counts detected in a 100 s interval as a function of the magnetic field of the 90° magnetic illustrated in fig. 1. A sample containing 10^{-12} $^{129}I/^{127}I$ was used.

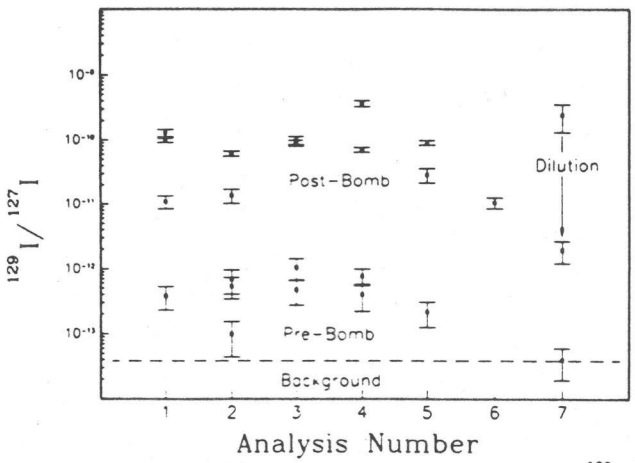

Fig. 3. A selected number of natural samples analyzed for ^{129}I is illustrated. Samples labeled post-bomb were derived from algae, sponges and corals. Those labeled pre-bomb were derived from old inland brines in addition to algae, seaweed and corals that predate 1942.

extracted, by the addition of a carrier, from a layer of 65 Myr coal-like material expected to have ground-water averages below $^{129}I/^{127}I$ of 10^{-12}. The origin of this anomalously high $^{129}I/^{127}I$ is as yet unknown ad remains the object of speculation [21] until a more detailed statigraphic analysis can be completed.

The choice of charge state 5 + ions was somewhat arbitrary and linked to the historical need to reduce the ion magnetic rigidity. In principal 4 + charge state ions would not have M/q and E/q ambiquities that could not be resolved by the high-resolution magnet. A threefold increase in the detection sensitivity would also be possible due to the increase yield of 4 + ions over 5 −

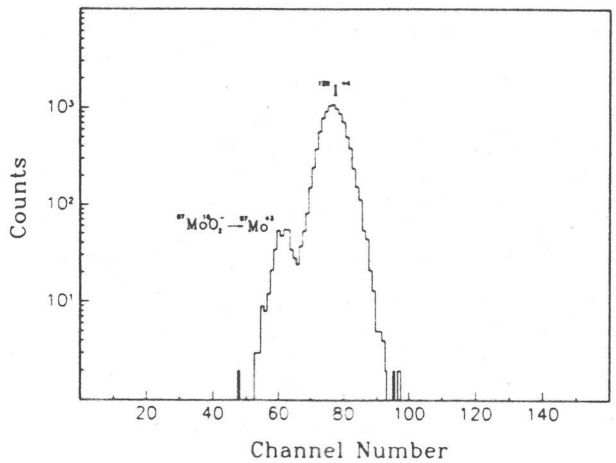

Fig. 4. An energy spectrum of counts from a surface barrier detector is illustrated for an AgI sample enriched in ^{129}I. The ^{97}Mo ions enter the detector as a result of a broadening of the ion energy distribution due to Coulomb explosion of the molecular ion oxide within the residual gas of the accelerator stripper canal.

ions. As the energy spectrum in fig. 4 illustrates, the $^{129}I^{4+}$ ions cannot be completely resolved from an interference produced by the $^{97}Mo^{3+}$ ions. These molecular fragments are generated by the acceleration and fragmentation of $^{97}MoO_2^-$. This result was unexpected as the mass resolving power of the analyzing magnet exceeded that required to resolve the ^{97}Mo by a factor of 8. A subsequent magnet scan of the ^{97}Mo ions when compared to a similar scan for ^{127}I revealed a factor of two increase in the Mo-ion momentum spread. This is consistent with an expected energy distribution that would result from Coulomb explosion of the molecule within the stripper gas. To benefit from the 4 + charge state, a higher resolution energy detector with reduced pulse height defect must be used.

5. Trace-element analysis

Previous studies have demonstrated the feasibility of determining the precious-metal content in a wide variety of materials by AMS [22–24]. Typically, the average bulk concentration was determined by dissolution of rock into a NiS melt, although pressed powder samples were also used. This has now been extended to the in situ measurement of the precious elements Au, Pt, Ir, Os, Ag, Pd, Rh and Ru within polished mineral grains within the host rock. Spot analysis of grain surfaces is important for the determination of the partitioning of PGE's between minerals, in particular between sulphides and silicates. As PGE's readily dissolve into sulphides, the subsequent segregation and accumulation of only a small amount of sulphide can produce a significant ore deposit. This calls for a need to determine the precious-metal content of different sulphides and their silicate interface with detection limits of sub-ppb, for both economic and research purposes.

The sample format is novel in that the analysis could be easily made from polished thin-section offcuts cored to produce a 4.5 mm diameter samples with no subsequent processing. The various minerals on each core were then probed using a 0.5 mm diameter Cs ion beam to determine the precious-metal distributions among the mineral grains [25,26]. The successful application of milliprobe analysis on mineral grains with AMS has bridged the gap between the high spatial resolution microprobe analysis techniques, with low-abundance parts per million (ppm) detection limits and the higher sensitivity low spatial resolution NAA or ICPMS techniques.

A particular simplification occurs if sulphides are chosen, as these minerals have relatively high electrical conductivity and therefore the problem of sample charging which had been a troublesome characteristic of previous measurements on some silicates and powders was avoided. Standardization was also relative simple as most reference materials were produced in the form of NiS beads with trace quantities of precious metals. Detection limits below 0.1 parts per billion (ppb) for Au and Ag were easily obtained.

Fig. 5 illustrates a correlation diagram of the measured precious-metal content of the reference material

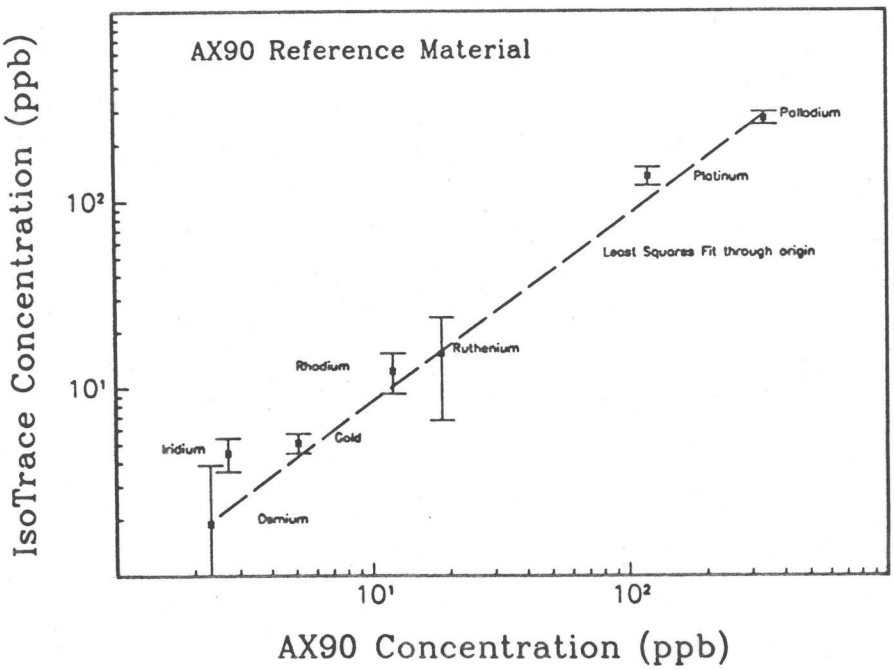

Fig. 5. The measured concentration of precious metals, normalized with respect to the SARM 7 "standard" is plotted against the expected concentration in the AX 90 reference material. The dashed line represents a linear least-squares fit constrained to pass through the origin.

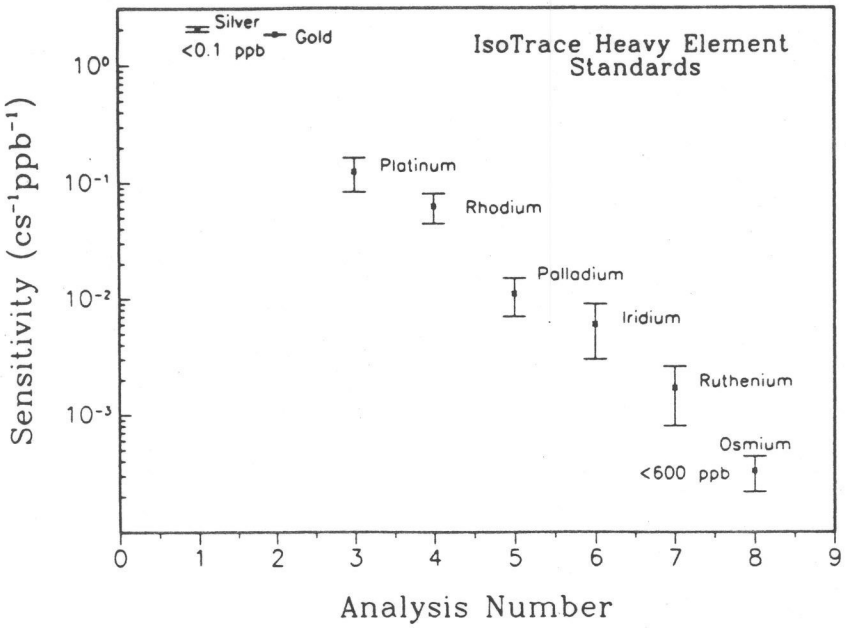

Fig. 6. The measured in situ precious metal sensitivity is plotted against an arbitrary measurement number for a combination of six reference materials. The detection limits at both extremes are the expected limits in a 500 s counting interval.

AX 90 [27] with respect to the AMS measurements normalized to SARM 7 [27], an accepted "standard" for precious metals. The least-squares fit was constrained through the origin and indicates a high degree of correspondence between the measured and expected concentrations. The abundances of platinum, gold and iridium were measured to be higher than the average concentration of metal. This was attributed to the unknown magnitude of the partition coefficients between the various components of the NiS beads, inhomogenei-

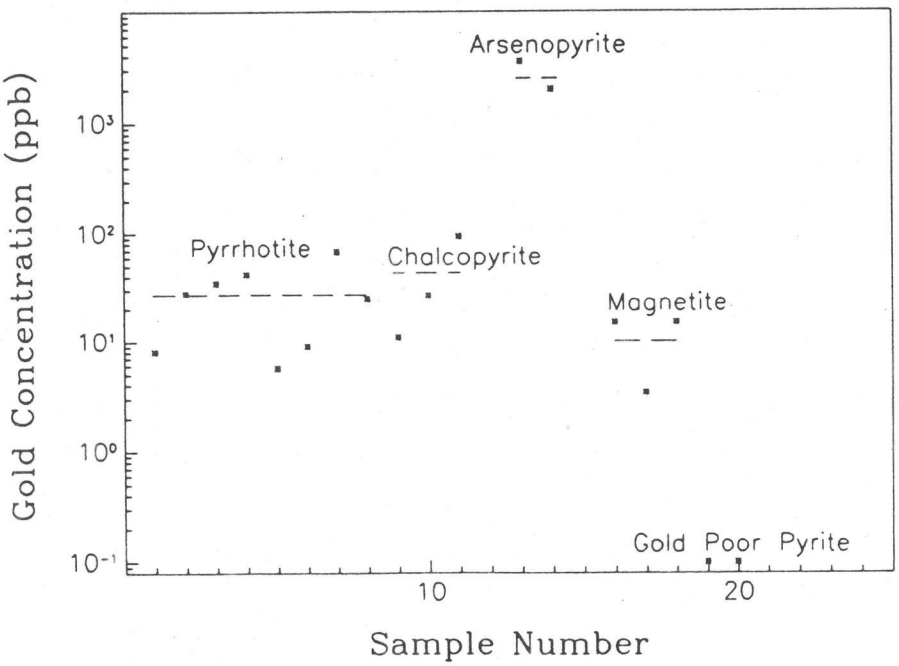

Fig. 7. The gold concentration for a selection of mineral grains from a gold-bearing ore are plotted as a function of analysis number. The gold-poor pyrite measurement was from a different material obtained from southeast Ontario.

ties and possible exsolution of precious metals into submicroscopic "blebs" which limit the ultimate attainable precision. Further study of sulphide matrix will be required and an analysis of other reference material has been undertaken.

The measured sensitivities for all these elements are summarized in fig. 6. Each point represents averages of the recorded counting rates of six standards, Sarm 7, AX 90, MRB-19, 21, 22 and 23 [27]. The apparent equality of gold and silver at 2 cps/ppb does not reflect the apparent difference in electron affinity as much as the differences in yield expected from the use of 6+ charge state for Au and 5+ for the silver ions. These sensitivities correspond to practical detection limits varying from 0.1 ppb for Ag and Au to 600 ppb for Os. The lower detection limits are also consistent with the "background" Pt and Au measured in a barren precious-metal-poor pyrite from the Chandos Lake area, southeast Ontario.

A typical ore analysis is illustrated in fig. 7, a composite of minerals analyzed for gold from within a gold-ore deposit in the province of British Columbia [26]. The arsenopyrite accounts for an appreciable fraction of the bulk gold assay. The apparent scatter in the gold concentrations of the other minerals is due to the analysis of different samples rather than the reproducibility on any one sample.

6. Negative-ion physics

The importance of negative-ion physics for AMS cannot be overstated. This is particularly true for heavy ions where absolute-Z information is not available, so that the instability of some negative-ion isobars provides the only practical means of separation from the ion of interest. The physics of weakly-bound negative ions is especially interesting as the theoretical techniques now exist to predict the possible ground-state configurations with sufficient accuracy [28].

The lack of a positive binding energy for the inert gases has always been attributed to the belief that closed shell atoms generally would not bind an additional electron to their ^1S ground states. It was for this reason that the other 11 closed shell elements (Be, Mg, Ca, Zn, Sr, Pd, Cd, Ba, Yb, Hg and Ra) were previously thought to have no bound negative-ion states. This was subsequently discovered to be incorrect. Pd is also an exception to the rule with an electron affinity of 0.558 eV. In recent trace element measurements [29] an anomalously high yield of Pd^- was observed. This may be indicative of a negative-ion formation where the excited state structure of the parent neutral atom that is sputtered plays a significant role in the formation of the negative ion. There is also some evidence that Zn^- would be bound by 0.090 eV in the $^2S_{1/2}$ state [30].

Although Be and Mg have no bound ground-state negative ions, Be^- has a ^4P metastable state of 10^{-4} s and Mg has a similar quartet state with a half-life of less than 10^{-8} s. Recently an analogous ^4P metastable state has been observed in Ca^{*-} with a 0.29 ms half-life [31] and Ca^- was found to be bound by 43 meV [32]. The group IIa element negative ions are of particular interest as the common belief prior to the discovery of the stable Ca^- ion was that all the negative ions of this group would be unbound. Calculations by Fischer and Vosko [28] indicated that this was not the case. Guided by the evidence that the lowest states of Sc^- and Y^- ions prefered $3d4s^24p$ and $4d5s^25p$ odd-parity states rather than filling the d orbital, as would be expected from the neighbouring group IIb $(n-1)dns^2$, their calculations indicated that the correlation energy provided by the addition of an electron to the p orbital was sufficiently large to overcome the negative binding of the ground state and relativistic energy components.

The ability to resolve alkaline elements injected as a result of fragmenting hydrides from the atomic negative ion cleared the way for a Sr and Ba negative-ion search. The complexity of hydride fragmentation and potential interference is clearly illustrated by the two-dimensional plot of the injected mass versus the post-accelerator analyzer mass spectrum from a sample of pure strontium shown in fig. 8. Similar scans for Ba and Ca confirm the existence of atomic negative ions resolved from the decay of a metastable hydride of the form MH_2^{*-} into MH^- [33,34].

The question of the magnitude of the electron affinity and the contribution from metastable ions remains a more difficult problem to resolve. The work function at the surface is a strongly dependent function of the oxygen to alkaline ratio [35] and as such would modulate the ion yield depending on the ion-source vacuum conditions. In all likelihood the observed ions have electron affinities that exceed 15 meV as they survived the electric gradients at the ion source and through the accelerator, both being approximately 1.0 MV/m. When mass-dependent effects are removed, the negative-ion yields observed indicate that both Sr^- and Ba^- are more strongly bound than Ca^-. Ba^- was also particularly abundant, arguing in favour of a possible significant contribution from excited states or even metastable ions.

7. The actinides and beyond

An analysis of actinide elements is made particularly difficult by a lack of electron-affinity data. Detailed calculations including relativistic corrections [36] indicate that for elements below Pu an extra electron will fill the 6d orbital with net positive, yet low binding energies. For Pu and above, the extra electron tends to

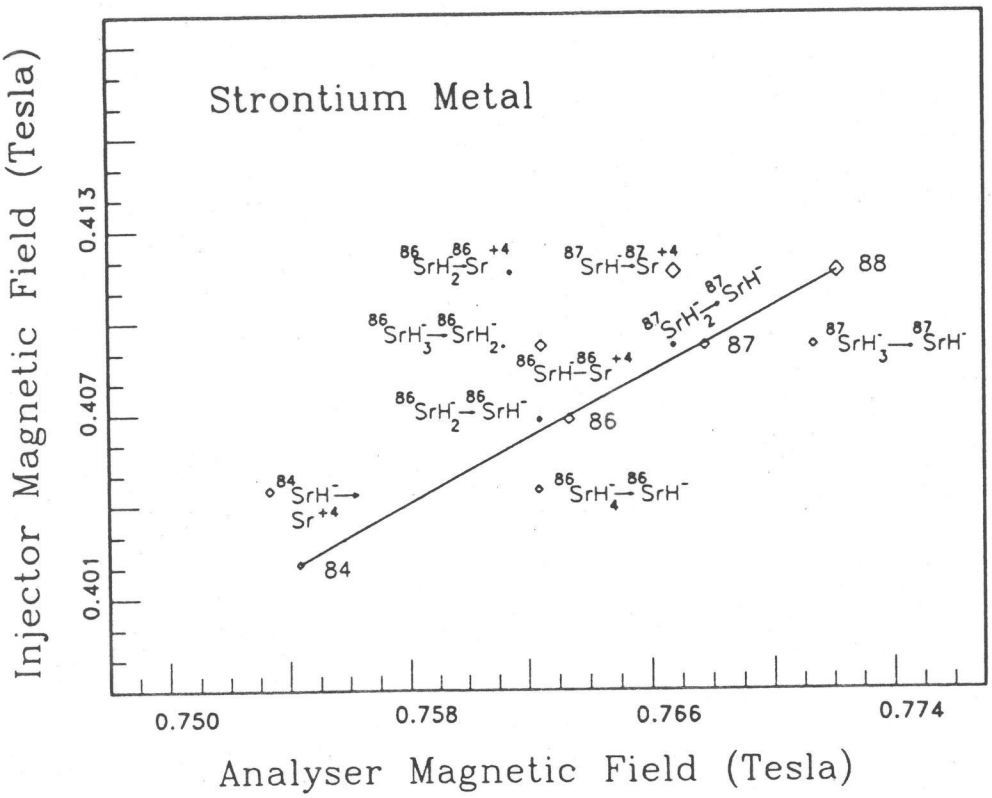

Fig. 8. The peak counting rates detected from a pure strontium metal sample are plotted as a function of the injection and post-accelerator magnetic fields. All the strontium isotopes originating as a negative ion fall along the indicated straight line determined from a measurement of ions known to produce negative ions. All stable and fragmenting metastable ion hydrides are clearly resolved from the strontium isotopes.

fill the 5f orbital. Relativistic effects which increase the shielding, tend to destabilize the additional f orbital electron thereby unbinding Pu^- and producing low ≤ 30 meV binding energies for Am and Cm. Fortunately Th has one of the highest binding energies within the actinides.

The U–Th decay series can be used as a chronometer on the time scale of 1000 kyr. Unlike the primarily divalent UO_2^{2+} ion, the tetravalent thorium ions are not easily dissolved in an oxidizing environment. Therefore the parent ^{234}U is removed from its source to start the radioisotope clock.

As thorium was observed to form negative ions and as no isobars exist, the $^{230}Th/^{232}Th$ ratio can be measured at low levels provided the molecular fragment interference can be removed. A sample of rich (40%) uranium ore was used for the initial search for ^{230}Th in natural materials as a high equilibrium abundance of 17 ppm was expected. Table 1 compares the measured $^{230}Th/^{232}Th$ ratios and the anticipated ratios in a variety of materials suspected of containing ^{230}Th. However, for routine actinide analysis by AMS, the use of molecules with the larger binding energies is indicated. For example UF_6^- has an electron affinity of near 5 eV.

Table 1
$^{230}Th/^{232}Th$ ratios tabulated for the expected and measured values in Th, U metals and U ore

	$^{230}Th/^{232}Th$	
	anticipated	measured
37% uranium ore	1.7×10^{-5}	1.6×10^{-5}
Th metal	origin dependent	6.0×10^{-6}
U metal	4.6×10^{-9}	2.5×10^{-10}

8. Conclusions

Although small accelerator systems are unlikely to replace completely the larger machines upon which AMS was initially developed, it is clear that significant analytical and research measurements can be made on a new generation of accelerators designed specifically for heavy-element analysis. The AMS of actinides, in particular ^{244}Pu, is relatively unexplored and may solve some long-outstanding problems such as the possibility of long-lived isotopes existing at the KT boundary as a result of nearby supernova or other impact debris.

References

[1] D. Elmore, P.W. Kubic, L.E. Tubbs, H.E. Gove, R. Teng, T. Hemmick, B. Chrunyk and N. Conard, Nucl. Instr. and Meth. B5 (1984) 109.

[2] M. Paul, D. Fink, G. Hollos, A. Kaufman, W. Kutschera and M. Magaritz, Nucl. Instr. and Meth. B29 (1987) 241.

[3] G. Korschinek, H. Morinaga, E. Nolte, E. Preisenberger, U. Ratzinger and A. Urban, Nucl. Instr. and Meth. B29 (1987) 67.

[4] L.R. Kilius, J.C. Rucklidge and A.E. Litherland, Nucl. Instr. and Meth. B29 (1987) 72.

[5] J.M. Antony and D.J. Donahue, Nucl. Instr. and Meth. B29 (1987) 77.

[6] M.-J. Nadeau and A.E. Litherland, these Proceedings (AMS 5) Nucl. Instr. and Meth. B52 (1990) 387.

[7] L.R. Kilius, M.-J. Nadeau, J.C. Rucklidge and A.E. Litherland, Nucl. Instr. and Meth. B29 (1987) 57.

[8] J. Heinemier, P. Hornshoj, H.L. Nielsen, N. Rud and M.S. Thomsen, Nucl. Instr. and Meth. B29 (1987) 110.

[9] W.M. Fairbank Jr., Nucl. Instr. and Meth. B29 (1987) 407.

[10] R.D. Evans, The Atomic Nucleus (McGraw-Hill, 1955).

[11] L.R. Kilius and A.E. Litherland, Nucl. Instr. and Meth. B26 (1987) 371.

[12] J.W. Wouters, D.J. Vieira, H. Wollnik, G.W. Butler, R.H. Kraus, Jr. and K. Vaziri, Nucl. Instr. and Meth. B26 (1987) 286.

[13] M.W Thompson, Nucl. Instr. and Meth. B18 (1987) 411.

[14] G. Doucas, Int. J. Mass Spect. and Ion Phys. 25 (1977) 71.

[15] L.R. Kilius, J.C. Rucklidge and A.E. Litherland, Nucl. Instr. and Meth B31 (1988) 433.

[16] M. Menat, Can. J. Phys. 42 (1964) 164.

[17] H.-D. Betz, Rev. Mod. Phys. 44 (1972) 465.

[18] D. Spence, W.A. Chopka and C.M. Stevens, J. Chem. Phys. 76 (1982) 2759.

[19] N. Baba, MSc Thesis, Dept. of Geology, University of Toronto, 1990.

[20] J. Fabrika-Martin, S.N. Davis and D. Elmore, Nucl. Instr. and Meth. B29 (1987) 361.

[21] G.E. Kocharov, these Proceedings (AMS 5) Nucl. Instr. and Meth. B52 (1990) 583.

[22] L.R. Kilius, J.C. Rucklidge, G.C. Wilson, H.W. Lee, K.H. Chang, A.E. Litherland, W.E. Kieser, R.P. Beukens and M.P. Gorton, Nucl. Instr. and Meth. B5 (1984) 185.

[23] J.C. Rucklidge, M.P. Gorton, G.C. Wilson, L.R. Kilius, A.E. Litherland, D. Elmore and H.E. Gove, Can. Mineral. 20 (1982) 111.

[24] S.H. Chew, T.J.L. Greenway and K.W. Allen, Nucl. Instr. and Meth. B5 (1984) 179.

[25] J.C. Rucklidge, G.C. Wilson and L.R. Kilius these Proceedings (AMS 5) Nucl. Instr. and Meth. B52 (1990) 507.

[26] G.C. Wilson, J.C. Rucklidge and L.R. Kilius, Suphidic zoned gold skarn mineralization at Rossland, British Columbia, Econ. Geol. (1990) to be published.

[27] G.C. Wilson, L.R. Kilius and J.C. Rucklidge, In situ, parts-per-billion analysis of precious metals in polished mineral samples and sulphide "standards" by accelerator mass spectrometry, submitted to Geochim. Cosmochim. Acta (1990).

[28] C.F. Fischer, J.B. Lagowski and S.H. Vosko, Phys. Rev. Lett. 59 (1987) 2263.

[29] J.C. Rucklidge, L.R. Kilius and G.C. Wilson, IsoTrace Internal Report.

[30] H.J. Kaiser, E. Heinicke, H. Baumann and K. Bethge, Z. Phys. 243 (1971) 46.

[31] D. Hanstorp, P. Devynck, W.G. Graham and J.R. Peterson, Phys. Rev. Lett. 63 (1989) 368.

[32] D.J. Pegg, J.S. Thomson, R.N. Compton and G.D. Alton, Phys. Rev. Lett. 59 (1987) 2267.

[33] L.R. Kilius, M.A. Garwan, A.E. Litherland, M.-J. Nadeau, J.C. Rucklidge and X.-L. Zhao, Nucl. Instr. and Meth. B40/41 (1989) 745.

[34] M.A. Garwan, A.E. Litherland, L.R. Kilius, M.-J. Nadeau and X.-L. Zhao, these Proceedings (AMS 5) Nucl. Instr. and Meth. B52 (1990) 512.

[35] A.H. Sommer, in: Photoemissive Materials (Wiley, New York, 1968) p. 113.

[36] Y. Guo and M.A. Whitehead, Phys. Rev. A40 (1989) 28.